Response of biological production and air–sea CO2 fluxes to upwelling intensification in the California and Canary Current Systems

Article *in* Journal of Marine Systems · January 2013

DOI: 10.1016/j.jmarsys.2012.04.003

CITATIONS
49

READS
301

2 authors:

Zouhair Lachkar
New York University Abu Dhabi
67 PUBLICATIONS **2,483** CITATIONS

SEE PROFILE

Nicolas Gruber
ETH Zurich
466 PUBLICATIONS **55,604** CITATIONS

SEE PROFILE

Journal of Marine Systems 109–110 (2013) 149–160

Contents lists available at SciVerse ScienceDirect

Journal of Marine Systems

journal homepage: www.elsevier.com/locate/jmarsys

Response of biological production and air–sea CO_2 fluxes to upwelling intensification in the California and Canary Current Systems

Zouhair Lachkar *, Nicolas Gruber

Environmental Physics, Institute of Biogeochemistry and Pollutant Dynamics, ETH Zurich, Universitätstrasse 16, CH-8092 Zurich, Switzerland

ARTICLE INFO

Article history:
Received 15 June 2011
Received in revised form 16 March 2012
Accepted 4 April 2012
Available online 24 April 2012

Keywords:
Eastern Boundary Upwelling Systems
Biological production
Upwelling intensification
Air–sea CO_2 exchange
Canary Current System
California Current System

ABSTRACT

Upwelling-favorable winds have increased in most Eastern Boundary Upwelling Systems (EBUS) in the last decades, and it is likely that they increase further in response to global climate change. Here, we explore the response of biological production and air–sea CO_2 fluxes to upwelling intensification in two of the four major EBUS, namely the California Current System (California CS) and Canary Current System (Canary CS). To this end, we use eddy-resolving regional ocean models on the basis of the Regional Oceanic Modeling System (ROMS) to which we have coupled a NPZD-type ecosystem model and a biogeochemistry module describing the carbon cycle and subject these model configurations to an idealized increase in the wind stress. We find that a doubling of the wind-stress doubles net primary production (NPP) in the southern California CS and central and northern Canary CS, while it leads to an increase of less than 50% in the central and northern California CS as well as in the southern Canary CS. This differential response is a result of i) different nutrient limitation states with higher sensitivity to upwelling intensification in regions where nutrient limitation is stronger and ii) more efficient nutrient assimilation by biology in the Canary CS relative to the California CS because of a faster nutrient-replete growth rate and longer nearshore water residence times. In the regions where production increases commensurably with upwelling intensification, the enhanced net biological uptake of CO_2 compensates the increase in upwelling driven CO_2 outgassing, resulting in only a small change in the biological pump efficiency and hence in a small sensitivity of air–sea CO_2 fluxes to upwelling intensification. In contrast, in the central California CS as well as in the southern Canary CS around Cape Blanc, the reduced biological efficiency enhances the CO_2 outgassing and leads to a substantial sensitivity of the air–sea CO_2 fluxes to upwelling intensification.

1. Introduction

Equatorward winds along the eastern boundaries of the Atlantic and Pacific induce offshore surface Ekman transport and the upwelling of nutrient-rich water into the euphotic zone, thereby stimulating high phytoplankton growth and leading to some of the most productive marine ecosystems in the world (Carr, 2001; Carr and Kearns, 2003; FAO, 2009; Pauly and Christensen, 1995). The high planktonic productivity in Eastern Boundary Upwelling Systems (EBUS) supports a large net fixation and subsequent export of organic carbon, which compensates the upwelling of CO_2-rich water (Muller-Karger et al., 2005). This tends to make these systems much smaller sources of CO_2 to the atmosphere than expected on the basis of their upwelling (Chavez and Takahashi, 2007). These air–sea CO_2 fluxes are highly variable in space and time, reflecting the high variability in the coastal upwelling and the strong modulation of the air–sea CO_2 exchange by biology, temperature, and the lateral carbon fluxes (Arístegui et al., 2004; Cai et al., 2006; Hales et al., 2005). Overall, upwelling systems located in the mid to high latitudes tend to be overall small sinks with seasonally reversing air–sea CO_2 fluxes (Borges and Frankignoulle, 2002; Hales et al., 2005), whereas those in the low latitudes tend to be a net source of CO_2 to the atmosphere because of a more intense and permanent upwelling (e.g., Lefévre et al. (2002)).

While supporting extremely rich ecosystems, EBUS are vulnerable to various anthropogenic perturbations, such as upper ocean warming (Di Lorenzo et al., 2005; Roemmich and McGowan, 1995), ocean acidification (Feely et al., 2008; Gruber et al., submitted for publication; Hauri et al., 2009), ocean deoxygenation (Bograd et al., 2008), and their possible interactive effects (Gruber, 2011). A particularly important perturbation is the increase in upwelling favorable wind (Bakun, 1990), for which there is mounting evidence that it has occurred already over the 20th century in several EBUS (Gutiérrez et al., 2011; Leduc et al., 2010; McGregor et al., 2007; Mendelssohn and Schwing, 2002; Schwing and Mendelssohn, 1997; Shannon et al., 1992). This strengthening of the wind forcing has been related to a global warming-induced increase in the land–sea thermal gradient (Bakun, 1990), and is therefore projected to increase further in the future (Diffenbaugh et al., 2004; Snyder et al., 2003). Yet, the effects of this physical perturbation on marine ecosystems in EBUS are neither well understood nor well quantified. In particular, the question of how biological production

* Corresponding author. Tel.: +41 44 632 08 94.
E-mail address: zouhair.lachkar@env.ethz.ch (Z. Lachkar).

0924-7963/$ – see front matter © 2012 Elsevier B.V. All rights reserved.
doi:10.1016/j.jmarsys.2012.04.003

and air–sea CO_2 fluxes in these systems might respond to such enhanced wind forcing has not been addressed yet, but is the main subject of this paper.

While the high production in EBUS is driven to first order by the upwelling of nutrient-rich water to the surface (Allen, 1973; Brink, 1983), only about half of the variations in net primary production (NPP) across all EBUS can be explained by differences in upwelling favorable winds (Carr, 2001; Carr and Kearns, 2003; Gruber et al., 2011; Lachkar and Gruber, 2012; Thomas et al., 2001). Moreover, recent observed changes in primary production show at best a moderate correlation with changes in wind (Demarcq, 2009; Kahru et al., 2009), suggesting different sensitivities of production to upwelling changes in the different EBUS. Hence, a better understanding of what controls this sensitivity of production to upwelling favorable wind change is needed for predicting potential future productivity changes and the impacts this has on the air–sea exchange of CO_2. This will also be needed in order to better evaluate future changes in ocean acidification and ocean deoxygenation.

We will show that bottom-up limitation factors such as light and temperature, as well as the water residence time in the nearshore region modulate the biological response to wind increase in EBUS. We will also demonstrate how these changes in production exert a major control on the sensitivity of the net air–sea CO_2 fluxes to upwelling changes in EBUS. Of particular relevance is the change in the efficiency of the biological pump, i.e., the relative balance between the nutrients and carbon that are transported and mixed upward into the euphotic zone and the nutrients and carbon that are fixed into organic matter and exported downward again (Sarmiento and Gruber, 2006). An efficient biological pump tends to cause uptake of CO_2 from the atmosphere, while an inefficient pump tends to lead to strong outgassing (Gruber and Sarmiento, 2002). We will show that those regions whose primary and export production increase commensurably with the upwelling maintain their biological pump efficiency and hence experience little change in their net air–sea CO_2 balance. In contrast, the regions where primary and export production increase less strongly turn into substantial sources of CO_2 for the atmosphere as a result of their decreased pump efficiency.

To arrive at these results, we undertook a comparative modeling study contrasting two of the four major EBUS, namely the California Current System (California CS) and the Canary Current System (Canary CS). The comparison of these two upwelling systems provides a framework for developing a better understanding of the underlying dynamics of EBUS ecosystems in general. Moreover, the comparative modeling approach provides a means to investigate how a single model produces a range of ecological and biogeochemical responses under slightly different external forcings. Using a series of eddy-resolving simulations of the California CS and the Canary CS under different wind forcing scenarios, this study identifies the potential response of biological production and air–sea CO_2 fluxes to upwelling intensification in EBUS and quantifies the key governing processes that determine the magnitude of this response.

2. Methods

We employ here the same model setups for the California and Canary Current Systems as described by Lachkar and Gruber (2011), but augmented with an interactive carbon cycle module. These two model setups are based on the UCLA-ETH version of the Regional Ocean Modeling System (ROMS) (Shchepetkin and McWilliams, 2005) and build on previous versions (e.g. Gruber et al., 2006; Marchesiello et al., 2003). Both model grids have a horizontal resolution of 5 km and 32 vertical levels with surface refinement.

The ecological–biogeochemical model is a nitrogen-based NPZD model (Gruber et al., 2006) with a single phytoplankton functional group, parameterized to represent a diatom-like group. Previous studies have shown that when addressing one type of ecosystems (e.g., EBUS in this study), NPZD-type models can be as successful as multiple functional group models for reproducing bulk ecosystem properties such as chlorophyll and primary production (Friedrichs and Hofmann, 2001; Friedrichs et al., 2007). Detritus is split into two pools: a large one that sinks fast, and a small one that sinks slowly, i.e., that behaves similar to dissolved organic matter. The model considers a dynamic phytoplankton chlorophyll-to-carbon ratio (θ) which mimics photoacclimation in phytoplankton (Falkowski and Raven, 1997). The chlorophyll-to-carbon ratio depends on irradiance, nutrient availability and temperature following the model of Geider et al. (1997). It is highest under high temperature, low irradiance and nutrient replete conditions and lowest at high irradiance, low temperature and under nutrient-limiting conditions. This down regulation in θ occurs as the rate of the photosynthetic energy supply from light absorption exceeds the capacity to assimilate photosynthate for growth.

Net primary production (NPP) is limited in our model by the amount of photosynthetically available radiation (PAR), I, the concentrations of nitrate, N_n, and ammonium, N_r, temperature, T, chlorophyll-to-carbon ratio, (θ), and phytoplankton biomass, P, in the following manner:

$$\mathrm{NPP} = \gamma(N_n, N_r)\cdot\mu_P^{\max}(T, I, \theta)\cdot P \tag{1}$$

where $\gamma(N_n,N_r)$ is a non-dimensional nutrient limitation factor and $\mu_P^{\max}(T,I,\theta)$ is the temperature-dependent, light-limited growth rate under nutrient replete conditions. The nutrient limitation factor $\gamma(N_n,N_r)\leq 1$, is parameterized using the Michaelis–Menten equation, taking into account that ammonium is taken up preferentially over nitrate, and that its presence inhibits the uptake of nitrate by phytoplankton (Wroblewski, 1977). The maximum nutrient limitation corresponds to $\gamma(N_n,N_r)=0$ while nutrient-unlimited growth is indicated by $\gamma(N_n,N_r)=1$. We use an additive function weighted toward ammonium:

$$\begin{aligned}\gamma(N_n, N_r) &= \gamma(N_n) + \gamma(N_r)\\ &= \frac{N_n}{K_{N_n}+N_n}\frac{K_{N_r}}{K_{N_r}+N_r} + \frac{N_r}{K_{N_r}+N_r}\end{aligned} \tag{2}$$

where K_{N_n} and K_{N_r} are the half-saturation constants for phytoplankton uptake of nitrate and ammonium, respectively. The temperature-dependent, light-limited growth rate is given by:

$$\mu_P^{\max}(T, I) = \frac{\mu_P^T(T)\cdot\alpha_P\cdot I\cdot\theta}{\sqrt{\left(\mu_P^T(T)\right)^2 + (\alpha_P\cdot I\cdot\theta)^2}} \tag{3}$$

Table 1
Rates of phytoplankton biological sources and sinks (in day^{-1}) under modern and increased winds in the California CS. Data are averaged vertically over the euphotic zone and horizontally over the 300 km wide nearshore area.

Wind forcing	Growth rate	Grazing loss	Mortality	Coagulation	Net growth
Modern wind (control)	0.21	0.1	0.024	0.01	0.08
Wind stress × 1.5	0.25	0.13	0.024	0.01	0.1
Wind stress × 2	0.28	0.14	0.024	0.01	0.11

Table 2
Rates of phytoplankton biological sources and sinks (in day^{-1}) under modern and increased winds in the Canary CS. Data are averaged vertically over the euphotic zone and horizontally over the 300 km wide nearshore area.

Wind forcing	Growth rate	Grazing loss	Mortality	Coagulation	Net growth
Modern wind (control)	0.21	0.11	0.024	0.01	0.07
Wind stress × 1.5	0.24	0.12	0.024	0.01	0.09
Wind stress × 2	0.3	0.15	0.024	0.01	0.13

where α_P is the initial slope in the growth versus light relationship. The temperature-dependent growth rate $\mu_P^T(T)$ is parameterized using the relationship of (Eppley, 1972):

$$\mu_P^T(T) = \ln 2 \cdot 0.851 \cdot (1.066)^T \quad (4)$$

All model parameters are set identical for both the California CS and Canary CS configurations and are those listed in Table 1 of Gruber et al. (2006).

A carbon cycle module was added requiring the inclusion of three new state variables, i.e., dissolved inorganic carbon (DIC), alkalinity, and mineral $CaCO_3$, all of which are subject to physical transport and mixing, including sinking in the case of $CaCO_3$. DIC is modified by net community production (i.e., net primary production minus heterotrophic respiration), air–sea gas exchange and precipitation and dissolution of $CaCO_3$. The concentration of alkalinity is altered by nitrification, new production and the precipitation and dissolution of $CaCO_3$. The transformations of organic carbon are tied to those of organic nitrogen with a fixed C:N ratio 106:16, while the formation and dissolution of mineral $CaCO_3$ are linked to the formation of organic matter via a constant ratio of 0.07. Particulate organic carbon is not explicitly modeled, but linked to the cycling of particulate organic nitrogen with the same 106:16 ratio. Particulate inorganic carbon, i.e., mineral $CaCO_3$ sinks with a constant velocity of 20 m s^{-1} and has a linear dissolution rate of 0.0057 day^{-1}.

The CO_2 flux at the air–sea interface F_{CO_2} is determined as:

$$F_{CO_2} = K_0 \cdot K_w \cdot (pCO_2^s - pCO_2^a) \quad (5)$$

where K_0 is the CO_2 solubility in water. pCO_2^s and pCO_2^a are the partial pressures of CO_2 at the ocean surface and in the atmosphere, respectively. K_w is the gas transfer (piston) velocity calculated using a quadratic dependence on the wind speed following the classical formulation of Wanninkhof (1992):

$$K_w = a \cdot U_{10}^2 \cdot \sqrt{\frac{660}{Sc}} \quad (6)$$

where a is a constant coefficient set to 0.31 for long-term steady winds and consistent with a piston velocity in cm s^{-1}, U_{10} is the wind speed at 10 m in m s^{-1} and Sc the Schmidt number for CO_2 calculated from surface temperature following Wanninkhof (1992). Oceanic pCO_2 is calculated from DIC, alkalinity, temperature, salinity, and nutrients using the standard OCMIP carbonate chemistry routines (http://www.ipsl.jussieu.fr/OCMIP/phase3/simulations/NOCES/HOWTO-NOCES-3.html) and employing the first and second dissociation constants of carbonic acid of Mehrbach et al. (1973) as refitted by Dickson and Millero (1987).

In the California CS the domain extends in latitude from the middle of Baja California (28°N) to the Canadian border (48°N) (~2000 km) and about 1000 km in offshore direction, thus encompassing the entire California CS and its most energetic eddy region (Fig. 1a). The domain of the Canary CS extends in latitude from 10°N (latitude of the North Equatorial Current) to 43°N (north-west Iberia) and in longitude from 5°W to 30°W. This is about 3200 km in alongshore and 1500 to 2500 km in offshore direction, and it encompasses the entire Canary CS and its different subsystems (Fig. 1b).

Initial and boundary conditions for temperature, salinity and nitrate were taken from the World Ocean Atlas 2005, while those for DIC and alkalinity were based on the Global Ocean Data Analysis Project (GLODAP) data set (Key et al., 2004). In the upper ocean, a seasonal cycle was added to the GLODAP-based annual mean DIC and alkalinity fields on the basis of the monthly pCO_2 climatology of Takahashi et al. (2009) and a monthly climatology of surface alkalinity calculated using temperature and salinity following Lee et al. (2006).

The models were started from rest, then run for 10 years with climatological monthly forcing. Wind stress was taken from the QuikSCAT-based Scatterometer Climatology of Ocean Winds (SCOW) (Risien and Chelton, 2008). The surface heat and freshwater fluxes were derived from the Comprehensive Ocean–Atmosphere Data Set (COADS) (da Silva et al., 1994) and applied with a surface temperature and salinity restoring following the formulation of Barnier et al. (1995). The models spin up within about 5 years, permitting us to use the results from model years 6 through 10 for further analyses. In order to remove the model's internally generated interannual variability, we generally show and discuss the averages of these last 5 years.

The two model setups show reasonable skills in capturing both the annual mean as well as the seasonal cycle of observed surface chlorophyll, temperature and mixed layer depth distributions (cf. Lachkar and Gruber (2011)). This is to a substantial degree due to the fidelity of the physical model that is able to capture the most important physical processes in the two upwelling systems thanks to its eddy-resolving resolution and realistic representation of coastal topography. Nevertheless, the models exhibit a few shortcomings. First, modeled SST exhibit a cold bias of about 1 °C relative to AVHRR satellite data in most of the California CS as well as in the northern Canary CS. Second, the model substantially underestimates SeaWiFS's high values in the immediate nearshore and slightly overestimates it in the offshore. We currently lack high-resolution DIC, alkalinity, or pCO_2 climatologies to evaluate our model results with regard to the carbon cycle. Initial results from comparisons with the limited in-situ observations in the California CS suggest that the model is able to capture the main characteristics of the ocean carbon cycle dynamics as well (Gruber et al., submitted for publication; Hauri et al., 2009). These indicate an underestimation of surface ocean pCO_2 in the nearshore area, linked in part to our cold bias, and an overestimation in the offshore areas, linked to our underestimation of biological production there. While a more detailed assessment of the quality of our simulated carbon parameters is clearly necessary, we consider our results as acceptable, as the known biases are generally small. They are also of the same nature in both systems and go in the same direction.

To explore the effects of the intensification of upwelling-favorable winds on coastal productivity and air–sea CO_2 fluxes, we conducted for each upwelling system three experiments: a control simulation where the wind was left unperturbed and two sensitivity simulations where the wind stress was increased by a factor of 1.5 and 2.0, respectively. Since both meridional and zonal components of the wind stress are increased by the same factor, the wind stress curl changed by the same factor as well. Wind speed was increased as well, but since wind stress depends on the square of wind speed, the corresponding increases in windspeed amount to only around 20% and 40%, respectively. These perturbations are much larger than those expected in the future (order of 30–50% increase in the wind stress curl for a doubling of carbon dioxide concentration (Diffenbaugh et al., 2004; Snyder et al., 2003)) and are also of idealized nature. Thus the results of these experiments should not be viewed as predictions, but rather as sensitivity studies to explore the potential responses of biological production and air–sea CO_2 fluxes to changes in upwelling intensity. These idealized perturbations also permit to better determine how these responses differ between the two systems and to elucidate the key processes that govern these responses.

3. Response of biological production to upwelling intensification

In the control simulation under modern winds, simulated primary production (NPP) in the California CS has its maximum between 34°N and 38°N where it exceeds 15 mol C $m^{-2}yr^{-1}$ over the 300 km wide nearshore on average and drops to less than 8 mol C $m^{-2}yr^{-1}$ north of 43°N and south of 32°N (Fig. 2a). Larger north–south variability characterizes the simulated NPP in the Canary CS, with maximum levels of NPP south of Cape Bojador reaching up to 32 mol C $m^{-2}yr^{-1}$ around cape Blanc and low NPP ranging between 5 mol C $m^{-2}yr^{-1}$ and 10 mol C $m^{-2}yr^{-1}$ further north (Fig. 2b).

Biological production increases in both systems in response to increased winds, yet the magnitude of the NPP increase varies considerably

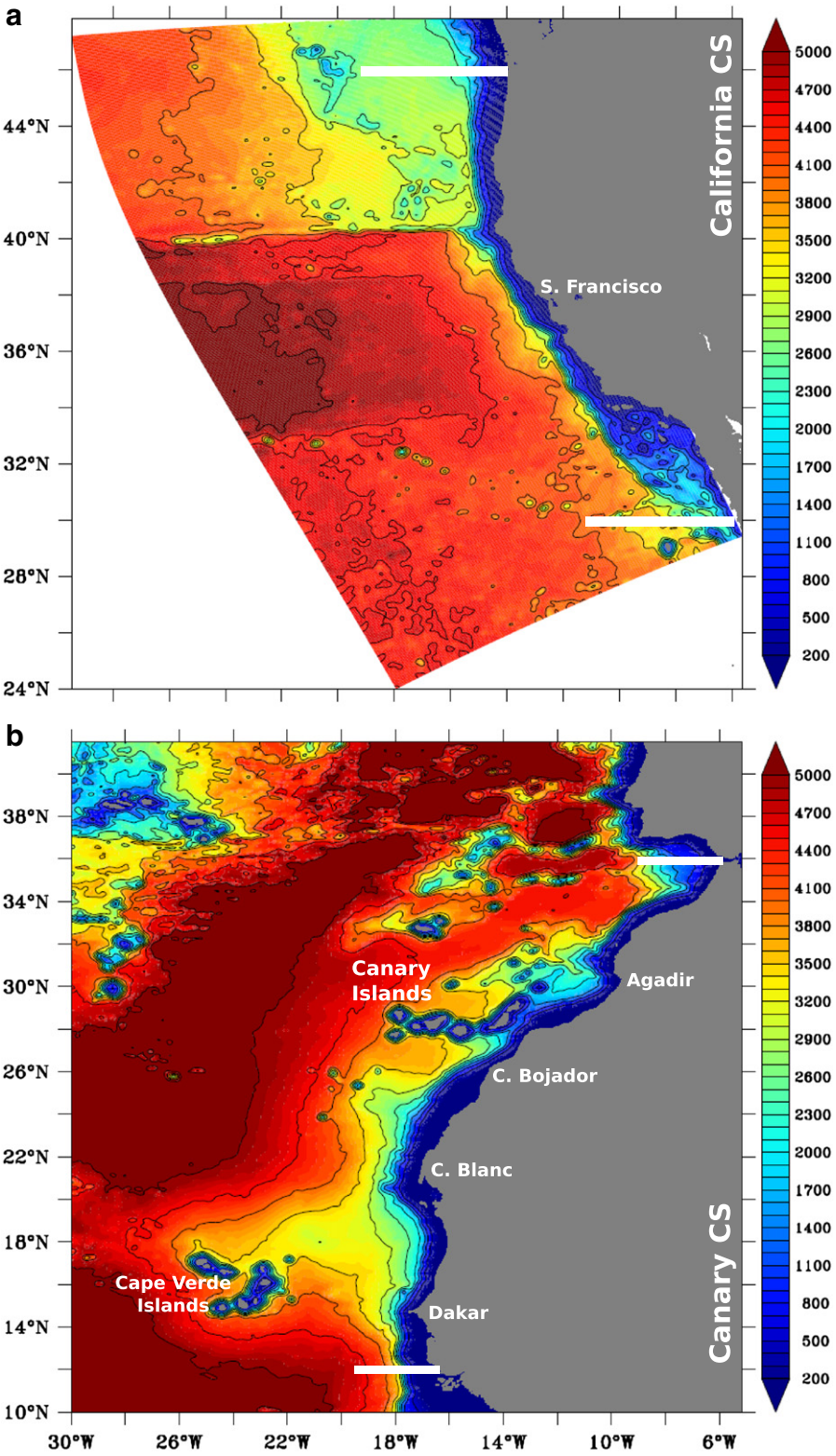

Fig. 1. Model domains for the California CS (top) and Canary CS (bottom) with the 2′ bathymetry ETOPO2 (Smith and Sandwell, 1997) in the background. The white segments indicate the northern and southern boundaries of the analysis area in each EBUS.

within and between the two upwelling systems (Fig. 2a–b). While NPP nearly doubles in the southern California CS as well as in the central and northern Canary CS in response to a doubling of the wind stress, NPP is only 15% to 50% higher in the central and northern California CS as well as in the southern Canary CS, i.e., south of Cape Blanc under the same wind perturbation (Fig. 2c–d). Such a large difference in the production response is surprising since the upwelling, and hence the potential supply of the limiting nutrients, increases everywhere by roughly the same factor.

First answers to this conundrum can be obtained by examining the factors that control primary production in our model (see Eq. (1)). Enhanced upwelling is expected to affect the first of the three drivers,

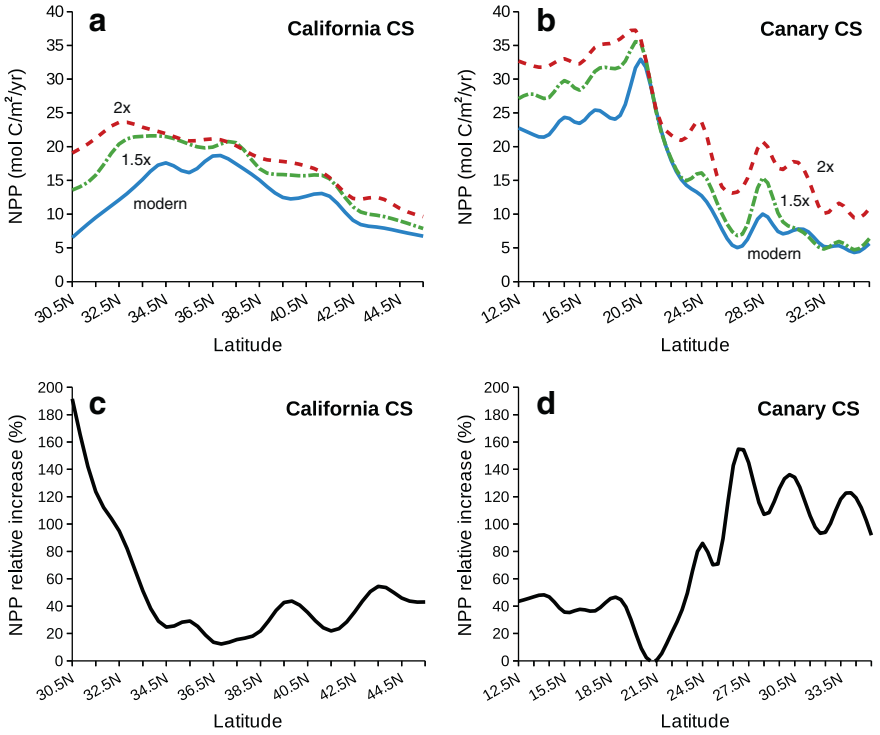

Fig. 2. (a)–(b) Meridional distribution of simulated NPP (mol C $m^{-2} yr^{-1}$) under modern winds (blue), 50% increased wind stress (green) and double wind stress (red), in the California CS and Canary CS. (c)–(d) Relative increase in NPP in the double wind stress simulation relative to the control simulations as a function of latitude in the California CS and Canary CS. NPP is vertically integrated over the euphotic zone and horizontally averaged over the 300 km wide nearshore area.

i.e., the nutrient limitation term $\gamma(N_n,N_r)$, as increased upwelling should lead to larger nutrient concentration in the euphotic zone. This is indeed the case, as the large NPP increases in the southern California CS and in the central and northern Canary CS are associated with substantial increases in $\gamma(N_n,N_r)$, i.e., decreases in the growth limitation by nutrients (Fig. 3). In contrast, the smaller productivity enhancements that

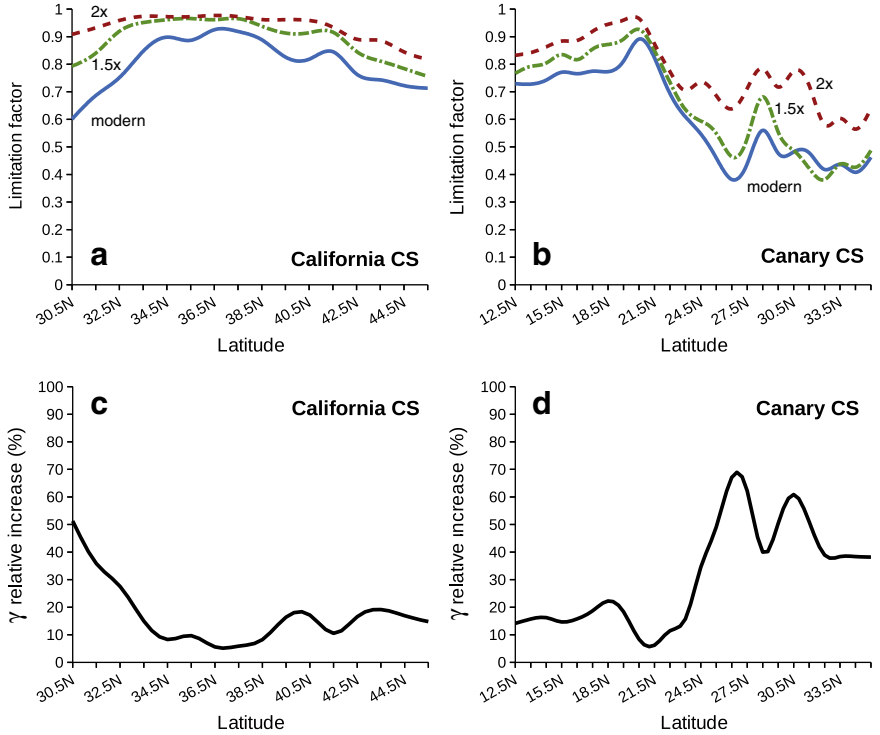

Fig. 3. (a)–(b) Meridional distribution of the nutrient limitation factor $\gamma(N_n,N_r)$ under modern winds (blue), 50% increased wind stress (green) and double wind stress (red) in the California CS and Canary CS. (c)–(d) Relative increase in $\gamma(N_n,N_r)$ in the double wind simulation relative to the control simulation as a function of latitude in the California CS and Canary CS. Data are vertically averaged over the euphotic zone and horizontally averaged over the 300 km wide nearshore area.

characterize the southern Canary CS as well as most of the California CS result from a more limited decrease in the nutrient limitation in these regions (Fig. 3). The relative changes in $\gamma(N_n,N_r)$ and NPP are highly correlated, with changes in nutrient limitation explaining 97% and 88% of the productivity increases in the California and Canary CS, respectively. The slope of the regression of the relative change in NPP versus the relative change in $\gamma(N_n,N_r)$ is nearly one, confirming that the NPP increases are primarily driven by changes in the nutrient limitation states. This strong relationship highlights at the same time that most of the variability in the magnitude of the changes can be understood by the very different initial nutrient limitation states: regions with low limitations tend to change little, while extended regions with strong nutrient limitations improve their nutrient limitation status and hence NPP substantially.

Overall, the decrease in nutrient limitation (increase in $\gamma(N_n,N_r)$) is larger in the Canary CS than in the California CS, i.e., 28% on average versus only 16% in the California CS. This occurs in spite of an overall larger increase in the nutrient content in the latter (Fig. 4). Euphotic layer inventory of total inorganic nitrogen TIN (i.e., nitrate and ammonium) increases by 70% in the California CS and only 34% in the Canary CS. A likely explanation is that since phytoplankton growth in most of the California CS is already close to saturation with respect to nutrient concentrations under modern winds ($\gamma(N_n,N_r)$ close to 1), phytoplankton is not able to keep up with the additional supply of nutrient resources, so that the inorganic nutrients remain untapped and accumulate in the euphotic zone. That is, with the exception of the southernmost and northernmost regions, most of the nearshore 300 km of the California CS is only weakly limited by nutrient availability. Therefore, upwelling intensification and the associated increase in the nutrient resources lead to a limited productivity enhancement in this upwelling system. In contrast, nutrient limitation is generally stronger in the Canary CS, particularly north of Cape Bojador, making this system more sensitive to upwelling intensification and the consequent increase in nutrient resources.

A closer look at the relationship between NPP and the nutrient limitation factor reveals a more complex story than one built only on the basis of bottom-up nutrient control. Fig. 5 shows that similar levels of nutrient limitation in the California CS and Canary CS are associated with substantially larger productivities in the latter, both under modern and increased winds. This indicates that for the same level of nutrients, the other two terms in the NPP equation (Eq (1)), i.e., the nutrient-replete growth rate $\mu_P^{max}(T,I,\theta)$ and the phytoplankton biomass P are much smaller in the California relative to the Canary CS. Lachkar and Gruber (2011) showed that the higher nutrient use efficiency in the Canary CS under modern winds is essentially driven by: i) a faster nutrient-replete growth rate due to more favorable light and temperature conditions and ii) the longer nearshore water residence times which permit a larger buildup of biomass. Next, we show that these findings remain valid under upwelling intensification scenarios.

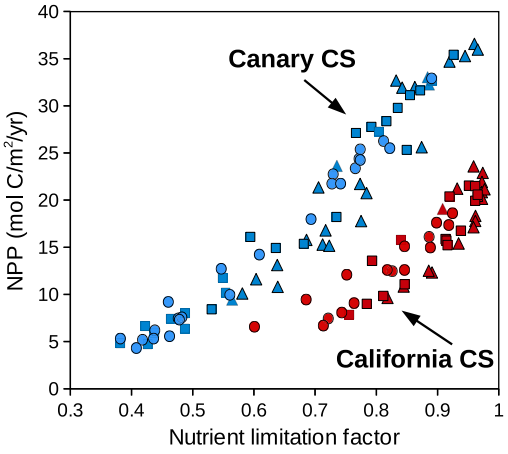

Fig. 5. NPP as a function of the nutrient limitation factor $\gamma(N_n,N_r)$ in the California CS (red) and Canary CS (blue) under modern winds (circles), 50% increased wind stress (squares) and double wind stress (triangles). Data were averaged over the 300 km wide nearshore area and over 1° bins in meridional direction.

4. The nutrient use efficiency in the California CS and Canary CS

In order to understand why nutrients are more efficiently used in the Canary CS relative to the California CS, we examine here the other drivers of productivity besides the availability of nutrients, that is, the nutrient-replete growth rate and phytoplankton biomass.

In the Canary CS, the simulated nutrient-replete growth rate $\mu_P^{max}(T,I,\theta)$ is on average around 0.37 day^{-1} ($\pm$0.1) under modern winds and slightly increases to 0.41 day^{-1} ($\pm$0.08) in the double wind stress simulation (Fig. 6). This increase in $\mu_P^{max}(T,I,\theta)$ is driven by a 25% increase in the chlorophyll-to-carbon ratio θ that results from larger nutrient concentrations in the euphotic zone under increased winds, and is partially compensated by the colder temperatures associated with the increased upwelling. In contrast, a lower average nutrient-replete growth rate of 0.29 day^{-1} ($\pm$0.05) characterizes the California CS both under unperturbed and increased winds (Fig. 6).

Phytoplankton biomass at a given location depends on the net growth, i.e., growth minus losses by grazing, coagulation and mortality, as well as transport and mixing, the net effect of which can be captured by the residence times in the nearshore area (Lachkar and Gruber, 2011). In all our simulations, net phytoplankton growth is essentially set by the balance between phytoplankton growth and grazing by zooplankton (see Tables 1 and 2). This is because coagulation and phytoplankton mortality terms are much smaller than the others and hence contribute very

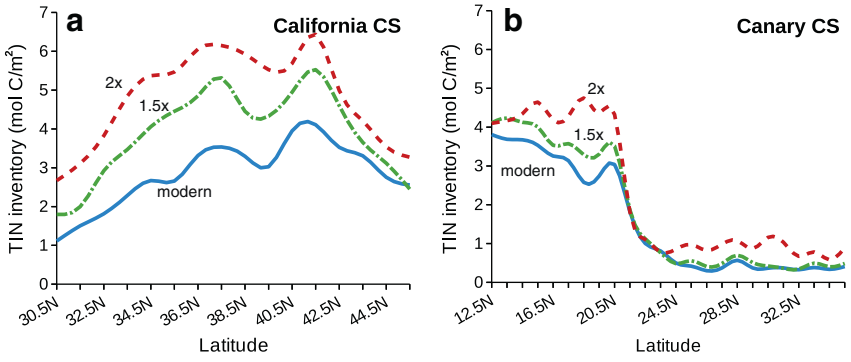

Fig. 4. Meridional distribution of Total Inorganic Nitrogen (TIN) inventory (mol C m^{-2}) in the California CS (left) and the Canary CS (right) under modern winds (blue), 50% increased wind stress (green) and double wind stress (red). Data are vertically integrated over the euphotic zone and horizontally averaged over the 300 km wide nearshore area.

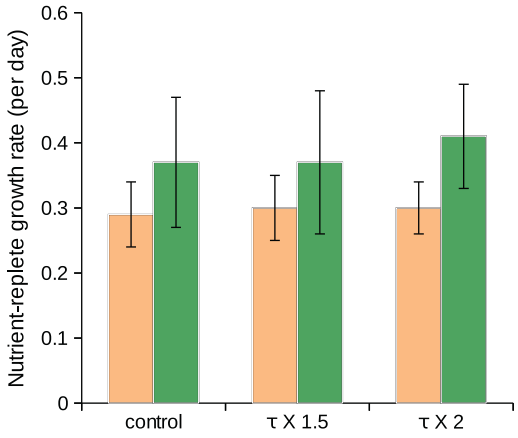

Fig. 6. Average nutrient-replete growth rate $\mu_P^{max}(T,I,\theta)$ (day^{-1}) in the California CS (orange) and Canary CS (green) under modern winds, 50% increased wind stress and double wind stress. Data are vertically averaged over the euphotic zone and horizontally over the 300 km wide nearshore area. The error bars indicate the meridional standard deviation in each upwelling system.

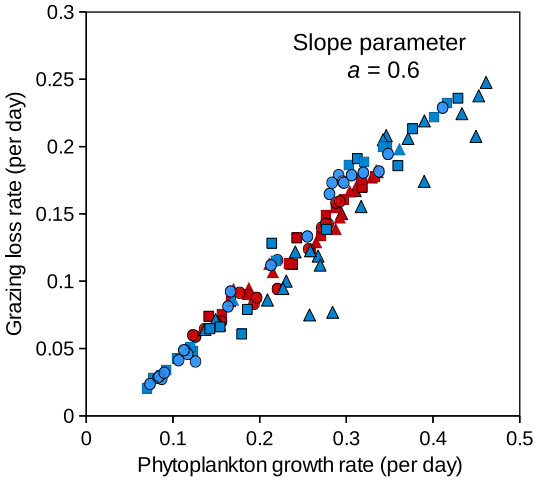

Fig. 7. The grazing loss as a function of the growth rate in the California CS (red) and Canary CS (blue) under modern winds (circles), 50% increased wind stress (squares) and double wind stress (triangles). Data were averaged vertically over the euphotic zone and horizontally over the 300 km wide nearshore area and over 1° bins in meridional direction.

little to net growth. The phytoplankton balance equation can therefore be written approximately as

$$\frac{\partial P}{\partial t} \approx \left(\mu_P - g_Z^{graz}\frac{Z}{K_P+P}\right)\cdot P + \Gamma_{trans}(P) \tag{7}$$

where μ_P is the total phytoplankton growth rate, g_Z^{graz} is the zooplankton grazing rate, K_P is the grazing half saturation constant, Z is the zooplankton biomass, and where $\Gamma_{trans}(P)$ is the transport operator of P, i.e., the net effect of advection and diffusion. This balance equation can be further simplified because it turns out that the rate of grazing loss, i.e., $g_Z^{graz}\frac{Z}{K_P+P}$ scales nearly linearly with the phytoplankton growth rate, μ_P, across both systems and irrespective of the magnitude of the winds (Fig. 7).

This strong coupling between phytoplankton growth and grazing rate results in our model from the interaction of the dynamics of zooplankton and that of total inorganic nitrogen (mainly ammonium). Given our model structure and parameter choices, the basal metabolism of zooplankton is the main sink process for zooplankton biomass and at the same time one of the most important source terms for TIN in the euphotic zone. This is because zooplankton mortality and remineralization of detritus are much smaller there. Therefore, in steady state, the zooplankton balance is given by zooplankton metabolism being equal to zooplankton growth by grazing and physical transport, while the TIN balance is given by the uptake by phytoplankton growth balancing zooplankton metabolism and physical transport. This gives for the euphotic zone the following two balances:

$$\Gamma_{trans}(Z) \approx g_Z^{graz}\beta_Z^{assim}\, Z\frac{P}{K_P+P} - \eta_Z^{meta}Z \tag{8}$$

$$\Gamma_{trans}(\mathrm{TIN}) \approx -\mu_P\cdot P + \eta_Z^{meta}Z \tag{9}$$

where β_Z^{assim} is the zooplankton assimilation efficiency and η_Z^{meta} the basal metabolism rate. Since the physical transport tends to affect the concentrations of zooplankton and TIN proportionally, i.e., $\Gamma_{trans}(Z) \propto \Gamma_{trans}(\mathrm{TIN})$, we can combine the two equations to yield the diagnosed proportionality of phytoplankton growth and zooplankton grazing.

This tight relationship between growth and grazing permits us to further simplify the phytoplankton balance Eq. (7) with good approximation to:

$$\frac{\partial P}{\partial t} \approx (1-a)\cdot\mu_P\cdot P + \Gamma_{trans}(P) \tag{10}$$

where a is the slope of the relationship between the grazing loss rate and the growth rate. This means that in steady-state, phytoplankton biomass would be governed by a relatively simple balance between the phytoplankton growth rate and the transport divergence as approximated by the water residence time as discussed by Lachkar and Gruber (2011).

Using a Lagrangian trajectory computation tool (Blanke and Raynaud, 1997) to evaluate water mass residence times, we found that the newly upwelled water masses stay more than 80% longer in the nearshore area in the Canary CS relative to the California CS (Fig. 8). These differences between the two systems change little under the upwelling intensification scenario. The longer water residence time in the Canary CS relative to the California CS likely results from the contrasting shelf widths and levels of eddy activity between the two systems (Gruber et al., 2011; Lachkar and Gruber, 2011). The wider continental shelf in the Canary CS results in an offshore displacement of the upwelling cell, producing an area over the innershelf where the circulation has almost no cross-shore transport (Marchesiello and Estrade, 2009). This prevents coastal water from being advected offshore, increasing the water residence time in the inner-shelf region. The higher level of eddy activity in

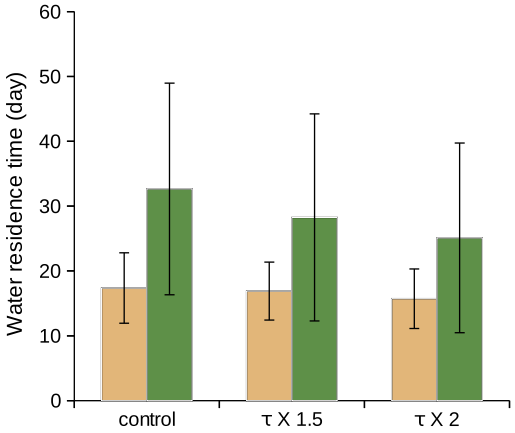

Fig. 8. Average water residence times in the 100 km wide nearshore area (day) in the California CS (orange) and Canary CS (green) under modern winds, 50% increased wind stress and double wind stress. Data are vertically averaged over the euphotic zone and horizontally over the 300 km wide nearshore area. The error bars indicate the meridional standard deviation in each upwelling system.

the California CS may also play an important role in reducing the water residence times in the coastal region of this system because of a higher eddy-induced subduction and offshore transport (Gruber et al., 2011).

In summary, the stronger nutrient limitation in the southern Californa CS and central and northern Canary CS makes the biological production in those regions more sensitive to upwelling intensification and associated increase in nutrient resources. Conversely, the quasi nutrient-replete conditions that characterize the central California CS and to a lesser extent the southern Canary CS result in a substantially lower sensitivity of production to enhanced upwelling in these regions. The different nutrient limitation states are insufficient to explain, however, the contrasting levels of production between the two upwelling systems both under modern and increased winds. That is, comparable levels of nutrient limitation in the California CS and Canary CS are generally associated with substantially larger productivity in the latter. This is due to a faster nutrient-replete growth rate and longer near-shore water residence times relative to the California CS both under modern and increased winds. In contrast, top-down control by zooplankton grazing appears to be very similar between the two systems, therefore not contributing to the differences in productivity.

Next, we explore the implications this has on the efficiency of the biological pump of carbon and the effects of upwelling intensification on the air-sea carbon exchange in the two upwelling systems.

5. Effect of upwelling intensification on the air–sea CO_2 exchange

The air–sea CO_2 fluxes not only react more strongly to upwelling intensification compared to biological production but also exhibit more regional differences in their responses (Fig. 9). The largest changes in the CO_2 fluxes occur in the central California as well as in the southern Canary CS along the Mauritanian Coast, where a wind stress increase of 50% tends to enhance the CO_2 outgassing by around 200% and a doubling increases the flux by a factor of 4 to 6. In contrast, in the central and northern Canary CS as well in the southernmost and northernmost California CS, upwelling intensification has nearly no effect on the air–sea CO_2 fluxes.

To understand this pattern of sensitivity of the air–sea CO_2 fluxes to upwelling intensification, we need to look at the changes in the biological pump efficiency (Sarmiento and Gruber, 2006) and also the changes in the air–sea gas transfer rate resulting from increased piston velocity under stronger windspeed (Eq (6)). The temperature driven CO_2 flux changes turn out to be small and will not be further investigated. To identify and understand the contribution of the change in the biological pump efficiency, we need to quantify the relative role of the two main processes governing this efficiency, i.e., i) the changes in upwelling that bring more waters with high CO_2 concentrations to the surface, and ii) the changes in the biology-driven drawdown of CO_2 near the surface and subsequent export of the produced organic carbon.

To separate these two factors and the contribution of the windspeed, we undertook a series of additional simulations. First, to separate the effect of biology on the air–sea CO_2 fluxes from that of circulation, we compare for each EBUS two abiotic simulations forced with modern winds and double wind stress to analogous simulations where biology is taken into account. Second, to evaluate the effect of increased gas transfer rate, we made for each upwelling system two additional simulations with and without biology, forced with double wind stress while keeping the windspeed constant in the gas transfer equation. To reduce the computational cost, we made these additional sensitivity experiments at a slightly coarser resolution of 15 km. An important caveat in this separation is that it is only an approximation and one that works best within the inner part of the domain. This is because the distribution of the abiotic simulation in the deeper parts of the model and near the domain boundaries still reflects to a certain degree the presence of the biological pump. On the one hand this is because our 10 year simulations are too short for the system to achieve a complete new steady-state. On the other hand, this is due to the fact that we kept the lateral boundary conditions the same for all simulations.

Despite this caveat, these separation simulations for modern winds clearly reveal the strongly opposing tendencies of biology and circulation on the air–sea CO_2 fluxes in the near-shore regions (Fig. 10a–b). Were circulation to act in isolation, these regions would be very large sources of CO_2 to the atmosphere with fluxes as large as 6 mol C m^{-2} yr^{-1}. Net biological uptake of the upwelled CO_2 substantially opposes this tendency everywhere, causing an uptake flux of CO_2 as large as 4 mol C m^{-2} yr^{-1}. The degree of biological compensation, i.e., the ratio of biologically driven atmospheric CO_2 uptake to the circulation driven CO_2 outgassing is larger than 75% in most of the California CS as well as in the southern Canary CS (Fig. 10c–d). In the central and northern Canary CS, the biological compensation varies between 45% and 70%. Since the degree of biological compensation is closely related to the biological pump efficiency, these values also indicate that even for modern winds, the biological pump efficiency is quite low in several regions of the two EBUS.

In the double wind stress simulation, the enhanced upwelling increases the circulation contribution to the CO_2 outgassing by more than a factor of two in both EBUS, whereas the biology driven atmospheric CO_2 uptake increases by only 30% and 44% in the California CS and Canary CS, respectively (Fig. 11). This leads to a substantial reduction in the biological compensation, particularly in the central California CS where it drops from around 75% under modern winds to between 20% and 30% in the double wind stress experiment (Fig. 10). A similar halving of the degree of biological compensation characterizes most of the southern Canary CS. These substantial reductions in compensation go together

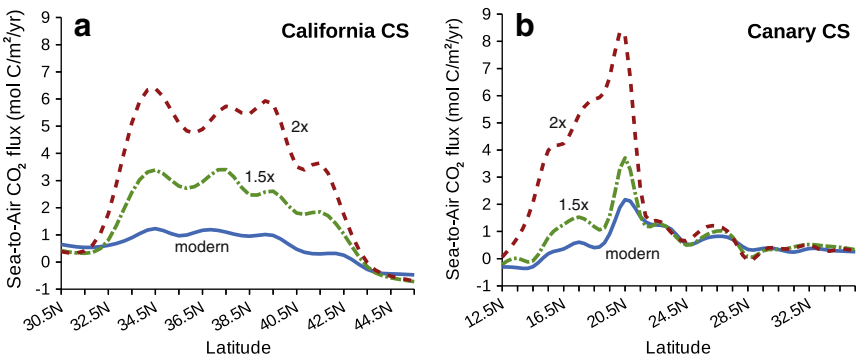

Fig. 9. Meridional distribution of simulated sea-to-air CO_2 flux (mol C m^{-2} yr^{-1}) in the California CS (left) and the Canary CS (right) under modern winds (blue), 50% increased wind stress (green) and double wind stress (red). Data are horizontally averaged over the 300 km wide nearshore area.

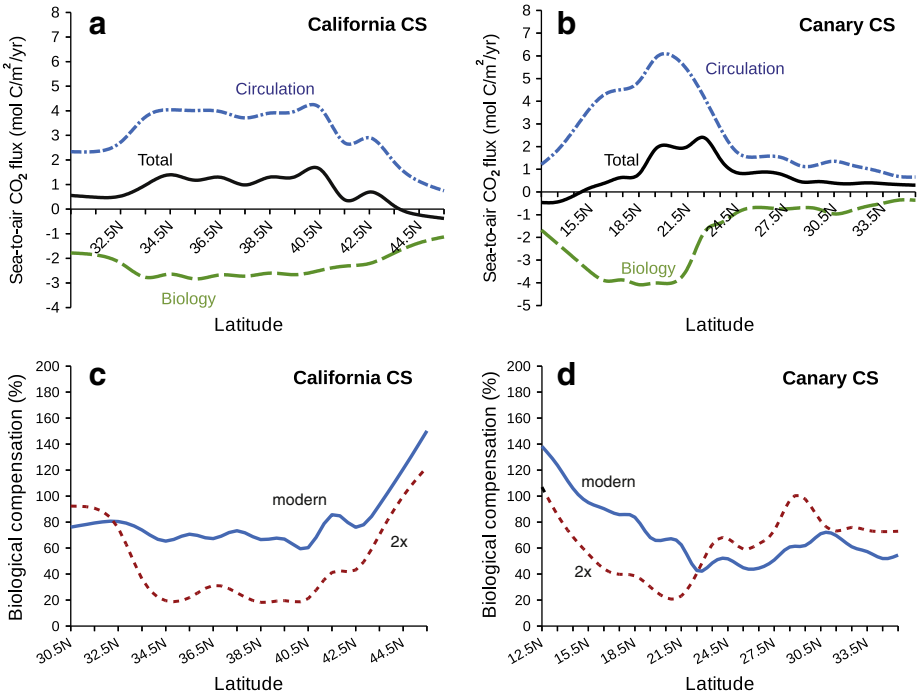

Fig. 10. (a)–(b) Decomposition of the simulated sea-to-air CO_2 flux under modern wind (black) into circulation driven (blue) and biology driven (green) components in the California CS (left) and Canary CS (right). (c)–(d) Degree of biological compensation (defined as the ratio of biology driven atmospheric CO_2 uptake to the physical circulation driven CO_2 outgassing) under modern winds (solid) and double wind stress (dashed), in the California CS (left) and Canary CS (right). The circulation component was computed based on an abiotic version of the model. The biology driven component is derived from the difference between the control simulation and the abiotic simulation. Data are horizontally averaged over the 300 km wide nearshore area.

with strong decreases in the biological pump efficiency. In contrast, enhanced upwelling leads to a slight increase in the degree of biological compensation and likely also pump efficiency in the northern Canary CS as well in the southernmost California CS.

The meridional distribution of the air–sea CO_2 flux anomaly drivers reveals the reasons for the large regional differences in the air–sea CO_2 flux response (Fig. 12). While the circulation changes enhance the CO_2 outgassing everywhere with the exception of one small region in the central Canary CS, the changes in biological production and export cause strong regional differences in the CO_2 outgassing response with both enhancing and reducing tendencies. The change in biologically-driven net carbon uptake reduces the outgassing north of Cape Bojador in the Canary CS and in the southernmost part of the California CS, whereas it enhances the outgassing in the central California CS and in the southern Canary CS. This enhancing effect of biology to the CO_2 outgassing is locally important and reaches up to 15% and 25% of the total anomalous CO_2 fluxes in the central California CS and in the southern Canary CS around Cape Blanc, respectively. Therefore, the large regional differences in the degree of biological compensation are driven more by regional differences in the biologically induced flux changes than by differences in the circulation driven flux changes.

The enhancing effect of biology on CO_2 outgassing in the central California CS and in the southern Canary CS is associated with a decrease in the vertical export production (i.e., the sum of the sinking and the physical export fluxes) in these regions under increased winds and hence a strong reduction in the efficiency by which inorganic carbon is

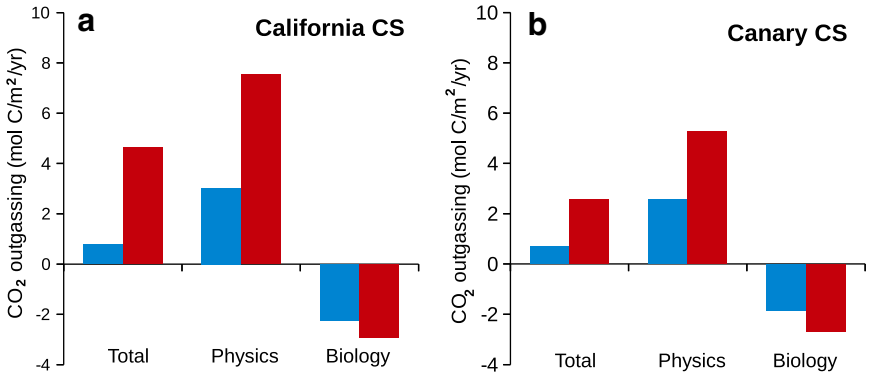

Fig. 11. Decomposition of the average sea-to-air CO_2 flux as simulated under modern wind (blue) and double wind stress (red) into circulation driven and biology driven components in the California CS (left) and Canary CS (right). The circulation component was computed based on an abiotic version of the model. The biology driven component is derived from the difference between the control simulation and the abiotic simulation. Data are horizontally averaged over the 300 km wide nearshore area.

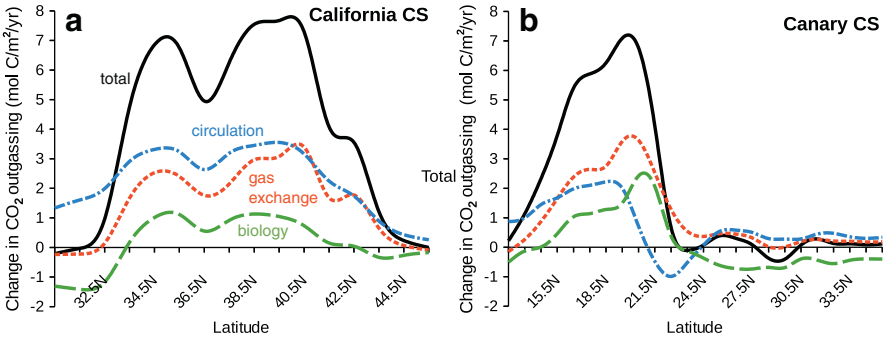

Fig. 12. Decomposition of the sea-to-air CO_2 flux increase under double wind stress into circulation (blue), biology (green) and gas exchange (orange) driven components in the California CS (left) and Canary CS (right). The gas exchange component is derived from the difference between the double wind stress experiment and an analogous simulation where the wind is held constant in the gas transfer formulation. Data are horizontally averaged over the 300 km wide nearshore area.

removed from the surface (Fig. 13). In contrast, in the northern Canary CS as well as in the southern California CS, the productivity increase is more important and is associated with an increase in the export production. This leads to a larger drawdown of carbon from the surface and compensates the effects of the circulation changes on the CO_2 outgassing fluxes. This results in an overall small sensitivity of the CO_2 fluxes to the upwelling intensification in these regions. An important caveat about the interpretation of the export fluxes is that we only considered here the vertical component of export, while an important fraction of organic matter is exported laterally.

So far, we have neglected the contribution of the changes in the CO_2 outgassing emanating from the increase in the gas transfer rate due to increased winds. It turns out that this factor contributes substantially to the enhanced fluxes, particularly in the Canary CS between 16°N and 22°N where it is responsible for 35% to 60% of the anomalous CO_2 flux, as well as in the central California CS where it represents between 35% and 45% of the total CO_2 outgassing increase. Nevertheless, the enhanced gas exchange appears to amplify rather than to cause the regional differences in the air–sea CO_2 flux responses (Fig. 12).

In summary, in most of the California CS as well as in the southern Canary CS around Cape Blanc, a limited increase in NPP is associated with a slight decrease in the carbon export and an overall decrease in the biology-driven CO_2 uptake. This lowers the biological pump efficiency and further enhances the CO_2 outgassing, thereby leading to a substantial sensitivity of the air–sea carbon exchange to the upwelling favorable wind increase. In contrast, the relatively large NPP increase in the northern Canary CS and southernmost California CS is associated with an important increase in the biology-driven uptake of CO_2 from the atmosphere. This compensates the effects of increased upwelling driven CO_2 outgassing, resulting in only a small sensitivity of air–sea CO_2 fluxes to upwelling intensification in these regions.

6. Summary and conclusions

We investigated the response of biological production and air–sea CO_2 fluxes to upwelling intensification in two of the four major EBUS, namely the California CS and the Canary CS. Our aim was to explore these responses and understand how and why they vary within and across the different EBUS.

We found on the basis of our model simulations that increased winds lead to a proportionally large production enhancement in the southern California CS and central and northern Canary CS, while the same wind perturbation results in a more limited increase in production in the central and northern California CS as well as in southern Canary CS. These differential responses result from i) different levels of nutrient limitation with higher sensitivity to upwelling intensification in regions where nutrient limitation is stronger and ii) more efficient nutrient use by biology in the Canary CS relative to the California CS because of a 25% faster nutrient-replete growth rate and nearly twice longer nearshore water residence times. These differences have consequences on the response of air–sea CO_2 fluxes to the upwelling intensification in both EBUS. In the southern California CS as well in the central and northern Canary, the large increase in production associated with upwelling intensification leads to an enhanced net biological uptake of CO_2. This compensates the increase in upwelling driven CO_2 outgassing, resulting in a small sensitivity of air–sea CO_2 fluxes to upwelling intensification. In contrast, in the central California CS as well as in the southern Canary CS around Cape Blanc, the reduced biological efficiency enhances the CO_2 outgassing

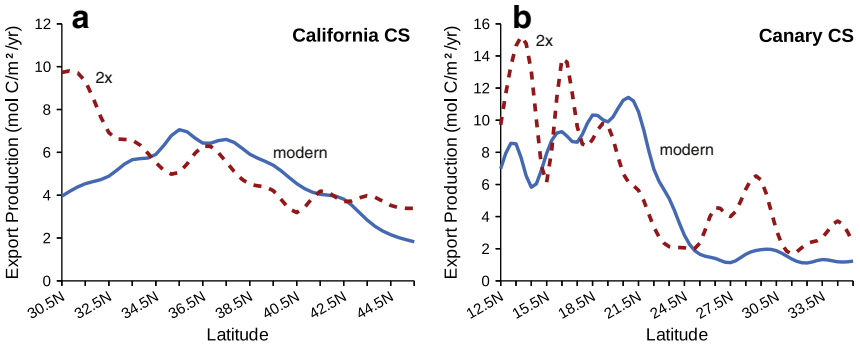

Fig. 13. Meridional distribution of export production (mol $C\,m^{-2}\,yr^{-1}$) in the subsurface (40 m) in the California CS (left) and the Canary CS (right) under modern winds (blue) and double wind stress (red). Data are horizontally averaged over the 300 km wide nearshore area.

and leads to a substantial sensitivity of the air–sea CO_2 fluxes to upwelling intensification.

Overall, our results illustrate how identical wind perturbations may lead to contrasting biological responses in EBUS characterized with only relatively modestly different physical and environmental conditions. More concretely, our comparative study shows that the biological response to upwelling intensification depends, in addition to the amplitude of the wind perturbation, on the initial nutrient conditions as well as factors controlling the biological growth and the nearshore-offshore water exchange.

Our study sheds light on the importance of physics and environmental conditions in shaping the sensitivity of these ecosystems to potential climate change induced upwelling-favorable wind intensification. Our study is limited with regard to the assessment of what implications the changes in productivity have on marine ecosystems and their food-web structure and on biogeochemical cycles beyond that of carbon and nitrogen. This would require the use of more complex biological models, in particular with regard to the explicit representation of multiple phytoplankton functional groups and different size classes of grazers. Such models would also permit to more fully document and predict potential taxonomic shifts and changes in the ecosystem structure that might impact the functioning of the biological pump and the carbon cycling in general in these systems. This clearly merits further in-depth investigation, something that we leave for future work.

We only addressed here the issue of increasing upwelling favorable wind and its potential impact on biological production in EBUS. Additional wind perturbations whose potential ecological impacts need to be considered include changes in the timing and the duration of the upwelling season (e.g., Barth et al., 2007) as well as impacts of upwelling intensification when they occur concomitant with surface warming and increasing vertical stratification (e.g., Rykaczewski and Dunne, 2010). Additional effects that need to be considered are upwelling driven changes in ocean acidification and coastal hypoxia.

Acknowledgments

Support for this research has come from the Swiss Federal Institute of Technology Zurich (ETH Zurich) and from the FP7 project CarboChange (Project reference 264879). Computations were performed at the central computing cluster of ETH Zurich, Brutus. We thank the ROMS developers in general, and particularly D. Loher and M. Münnich at ETH Zürich for their help and support. We are grateful to B. Blanke and N. Grima for making their ARIANE code available.

References

Allen, J., 1973. Upwelling and coastal jets in a continuously stratified ocean. J. Phys. Oceanogr. 3, 245–257.
Arístegui, J., Barton, E.D., Tett, P., Montero, M.F., Garcia-Muñoz, M., Basterretxea, G., Cussatlegras, A., Ojeda, A., de Armas, D., 2004. Variability in plankton community structure, metabolism, and vertical carbon fluxes along an upwelling filament (Cape Juby, NW Africa). Prog. Oceanogr. 62, 95–113, http://dx.doi.org/10.1016/j.pocean.2004.07.004.
Bakun, A., 1990. Global climate change and intensification of coastal ocean upwelling. Science 247, 198–201, http://dx.doi.org/10.1126/science.247.4939.198.
Barnier, B., Siefried, L., Marchesiello, P., 1995. Thermal forcing for a global ocean circulation model using a three-year climatology of ECMWF analyses. J. Mar. Syst. 6, 363–380.
Barth, J.A., Menge, B.A., Lubchenco, J., Chan, F., Bane, J.M., Kirincich, A.R., McManus, M.A., Nielsen, K.J., Pierce, S.D., Washburn, L., 2007. Delayed upwelling alters nearshore coastal ocean ecosystems in the northern California Current. PNAS 104 (10), 3719–3724.
Blanke, B., Raynaud, S., 1997. Kinematics of the Pacific equatorial undercurrent: an Eulerian and Lagrangian approach from GCM results. J. Phys. Oceanogr. 27, 1038–1053.
Bograd, S.J., Castro, C.G., Di Lorenzo, E., Palacios, D.M., Bailey, H., Gilly, W., Chavez, F.P., 2008. Oxygen declines and the shoaling of the hypoxic boundary in the California Current. Geophys. Res. Lett. 35, L12607, http://dx.doi.org/10.1016/S0967-0645(01)00094-7.
Borges, A.V., Frankignoulle, M., 2002. Distribution of surface carbon dioxide and air–sea exchange in the upwelling system off the Galician coast. Global Biogeochem. Cycles 16 (2), 1020, http://dx.doi.org/10.1029/2000GB001385.
Brink, K., 1983. The near-surface dynamics of coastal upwelling. Prog. Oceanogr. 12, 223–257, http://dx.doi.org/10.1016/0079-6611(83)90009-5.
Cai, W.-J., Dai, M., Wang, Y., 2006. Air–sea exchange of carbon dioxide in ocean margins: a province-based synthesis. Geophys. Res. Lett. 33, L12603, http://dx.doi.org/10.1029/2006GL026219.
Carr, M., 2001. Estimation of potential productivity in eastern boundary currents using remote sensing. Deep-Sea Res. II Top. Stud. Oceanogr. 49, 59–80, http://dx.doi.org/10.1016/S0967-0645(01)00094-7.
Carr, M., Kearns, E.J., 2003. Production regimes in four eastern boundary current systems. Deep-Sea Res. II Top. Stud. Oceanogr. 50, 3199–3221, http://dx.doi.org/10.1016/j.dsr2.2003.07.015.
Chavez, F.P., Takahashi, T., 2007. Coastal oceans. In: King, A.W., Dilling, L., Zimmerman, G.P., Fairman, D.M., Houghton, R.A., Marland, G.H., Rose, A.Z., Wilbanks, T.J. (Eds.), A Report by the U.S. Climate Change Science Program and the Subcommittee on Global Change Research. National Ocean and Atmospheric Administration, Climate Program Office, Silver Spring, MD, USA, pp. 83–92.
da Silva, A.M., Young, C.C., Levitus, S., 1994. Atlas of surface marine data 1994. Volume 1: Algorithms and Procedures. Technical Report NOAA Atlas NESDIS 6. National Oceanic and Atmospheric Administration, Washington, DC.
Demarcq, H., 2009. Trends in primary production, sea surface temperature and wind in upwelling systems (1998–2007). Prog. Oceanogr. 83, 376–385, http://dx.doi.org/10.1016/j.pocean.2009.07.022.
Di Lorenzo, E., Miller, A.J., Shneider, N., McWilliams, J.C., 2005. The warming of the California Current System: dynamics and ecosystem implications. J. Phys. Oceanogr. 35 (3), 336–362.
Dickson, A.G., Millero, F.J., 1987. A comparison of the equilibrium constants for the dissociation of carbonic acid in seawater media. Deep-Sea Res. I Oceanogr. Res. Pap. 34.
Diffenbaugh, N.S., Snyder, M.A., Sloan, L.C., 2004. Could CO_2-induced land-cover feedbacks alter near-shore upwelling regimes? Proc. Natl. Acad. Sci. U. S. A. 101, 27–32.
Eppley, R.W., 1972. Temperature and phytoplankton growth in the sea. Fish. Bull. 70, 1063–1085.
Falkowski, P.G., Raven, J., 1997. Aquatic Photosynthesis. Blackwell, Oxford. 375 pp.
FAO, 2009. The State of World Fisheries and Aquaculture 2008, Pap/Cdr edn. Food & Agriculture Org.
Feely, R.A., Sabine, C.L., Hernandez-Ayon, J.M., Ianson, D., Hales, B., 2008. Evidence for upwelling of corrosive "acidified" water onto the continental shelf. Science 320 (5882), 1490–1492, http://dx.doi.org/10.1126/science.1155676.
Friedrichs, M.A.M., Hofmann, E.E., 2001. Physical control of biological processes in the central equatorial Pacific Ocean. Deep Sea Res. Part I 48, 1023–1069.
Friedrichs, M.A.M., Dusenberry, J.A., Anderson, L.A., Armstrong, R.A., Chai, F., Christian, J.R., Doney, S.C., Dunne, J., Fujii, M., Hood, R., Mcgillicuddy, D.J., Moore, J.K., Schartau, M., Spitz, Y.H., Wiggert, J.D., 2007. Assessment of skill and portability in regional marine biogeochemical models: role of multiple planktonic groups. J. Geophys. Res. Oceans 112 (C8).
Geider, R.J., MacIntyre, H.L., Kana, T.M., 1997. Dynamic model of phytoplankton growth and acclimation: responses of the balanced growth rate and the chlorophyll a: carbon ratio to light, nutrient-limitation and temperature. Mar. Ecol. Prog. Ser. 148, 187–200.
Gruber, N., 2011. Warming up, turning sour, losing breath: ocean biogeochemistry under global change. Philos. Trans. R. Soc. London, Ser. A 369 (1943), 1980–1996.
Gruber, N., Sarmiento, J.L., 2002. Biogeochemical/physical interactions in elemental cycles. In: Robinson, A.R., McCarthy, J.J., Rothschild, B.J. (Eds.), The Sea: Biological–Physical Interactions in the Oceans, vol. 12. John Wiley and Sons, New York, pp. 337–399.
Gruber, N., Frenzel, H., Doney, S.C., Marchesiello, P., McWilliams, J.C., Moisan, J.R., Oram, J., Plattner, G.-K., Stolzenbach, K.D., 2006. Eddy-resolving simulation of plankton ecosystem dynamics in the California Current System. Deep Sea Res. Part I 53, 1483–1516, http://dx.doi.org/10.1016/j.dsr.2006.06.005.
Gruber, N., Lachkar, Z., Frenzel, H., Marchesiello, P., Munnich, M., McWilliams, J.C., Nagai, T., Plattner, G.-K., 2011. Mesoscale eddy-induced reduction of biological production in coastal upwelling systems. Nat. Geosci. 4, 787–792.
Gruber, N., Hauri, C., Lachkar, Z., Loher, D., Plattner, G.-K., submitted for publication. Rapid progression of ocean acidification in the California Current System. Science.
Gutiérrez, D., Bouloubassi, I., Sifeddine, A., Purca, S., Goubanova, K., Graco, M., Field, D., Méjanelle, L., Velazco, F., Lorre, A., Salvatteci, R., Quispe, D., Vargas, G., Dewitte, B., Ortlieb, L., 2011. Coastal cooling and increased productivity in the main upwelling zone off Peru since the mid-twentieth century. Geophys. Res. Lett. 38, L07603, http://dx.doi.org/10.1029/2010GL046324.
Hales, B., Takahashi, T., Bandstra, L., 2005. Atmospheric CO2 uptake by a coastal upwelling system. Global Biogeochem. Cycles 19, GB1009, http://dx.doi.org/10.1029/2004GB002295.
Hauri, C., Gruber, N., Plattner, G.-K., Alin, S., Feely, R.A., Hales, B., Wheeler, P.A., 2009. Ocean acidification in the California Current System. Oceanography 22 (4), 60–71, http://dx.doi.org/10.5670/oceanog.2009.97.
Kahru, M., Kudela, R., Manzano-Sarabia, M., Mitchell, B.G., 2009. Trends in primary production in the California Current detected with satellite data. J. Geophys. Res. 114, C02004.
Key, R.M., Lee, C.L.S.K., Wanninkhof, R., Bullister, J., Feely, R.A., Millero, F.J., Mordy, C., Peng, T.-H., 2004. A global ocean carbon climatology: Results from Global Data Analysis Project (GLODAP). Global Biogeochem. Cycles 18, GB4031, http://dx.doi.org/10.1029/2004GB002247.
Lachkar, Z., Gruber, N., 2011. What controls biological production in coastal upwelling systems? Insights from a comparative modeling study. Biogeosciences 8, 2961–2976, http://dx.doi.org/10.5194/bg-8-2961-2011.
Lachkar, Z., Gruber, N., 2012. A comparative study of biological production in eastern boundary upwelling systems using an artificial neural network. Biogeosciences 9, 293–308, http://dx.doi.org/10.5194/bg-9-293-2012.

Leduc, G., Herbert, C.T., Blanz, T., Martinez, P., Schneider, R., 2010. Contrasting evolution of sea surface temperature in the Benguela upwelling system under natural and anthropogenic climate forcings. Geophys. Res. Lett. 37 (L20705), 1–5.
Lee, K., Tong, L., Millero, F., Sabine, C., Dickson, A., Goyet, C., Geun-Ha, P., Wanninkhof, R., Feely, R., Key, R., 2006. Global relationships of total alkalinity with salinity and temperature in surface waters of the world's oceans. Geophys. Res. Lett. 33, http://dx.doi.org/10.1029/2006GL027207.
Lefévre, N., Aiken, J., Rutllant, J., Daneri, G., Lavender, S., Smyth, T., 2002. Observations of pCO^2 in the coastal upwelling off Chile: spatial and temporal extrapolation using satellite data. J. Geophys. Res. 107 (C6), 3055, http://dx.doi.org/10.1029/2000JC000395.
Marchesiello, P., Estrade, P., 2009. Eddy activity and mixing in upwelling systems: a comparative study of Northwest Africa and California regions. Int. J. Earth Sci. 98, 299–308, http://dx.doi.org/10.1007/s00531-007-0235-6.
Marchesiello, P., McWilliams, J.C., Shchepetkin, A.F., 2003. Equilibrium structure and dynamics of the California Current System. J. Phys. Oceanogr. 33, 753–783.
McGregor, H.V., Dima, M., Fischer, H.W., Mulitza, S., 2007. Rapid 20th-century increase in coastal upwelling off northwest Africa. Science 315, 637–639, http://dx.doi.org/10.1126/science.1134839.
Mehrbach, C., Culberson, C., Hawley, J., 1973. Measurement of the apparent dissociation constants of carbonic acid in seawater at atmospheric pressure. Limnol. Oceanogr. 18, 897–907.
Mendelssohn, R., Schwing, F.B., 2002. Common and uncommon trends in SST and wind stress in the California and Peru–Chile current systems. Prog. Oceanogr. 53, 141–162, http://dx.doi.org/10.1016/S0079-6611(02)00028-9.
Muller-Karger, F.E., Varela, R., Thunell, R., Luerssen, R., Hu, C., Walsh, J.J., 2005. The Importance of Continental Margins in the Global Carbon Cycle.
Pauly, D., Christensen, V., 1995. Primary production required to sustain global fisheries. Nature 374, 255–257, http://dx.doi.org/10.1038/374255a0.
Risien, C.M., Chelton, D.B., 2008. A global climatology of surface wind and wind stress fields from eight years of QuikSCAT scatterometer data. J. Phys. Oceanogr. 38, 2379–2413.
Roemmich, D., McGowan, J., 1995. Climatic warming and the decline of zooplankton in the California current. Science 267 (5202), 1324–1326.
Rykaczewski, R.R., Dunne, J.P., 2010. Enhanced nutrient supply to the California Current ecosystem with global warming and increased stratification in an earth system model. Geophys. Res. Lett. 37, L21606, http://dx.doi.org/10.1029/2010GL045019.
Sarmiento, J.L., Gruber, N., 2006. Ocean Biogeochemical Dynamics. Princeton University Press.
Schwing, F.B., Mendelssohn, R., 1997. Increased coastal upwelling in the California Current System. J. Geophys. Res. 102 (C2), 3421–3438, http://dx.doi.org/10.1029/96JC03591.
Shannon, L., Crawford, R., Pollock, D., Hutchings, L., Boyd, A., Taunton-Clark, J., Badenhorst, A., Melville-Smith, R., Augustyn, C., Cochrane, K., Hampton, I., Nelson, G., Japp, D., Tarr, R., 1992. The 1980s a decade of change in the Benguela ecosystem. S. Afr. J. Mar. Sci. 12, 271–296.
Shchepetkin, A.F., McWilliams, J.C., 2005. The regional oceanic modeling system (ROMS): a split-explicit, free-surface, topography-following-coordinate oceanic model. Ocean Modell., IX. Hooke Inst. Oxford Univ., Oxford, U. K., p. 347404.
Smith, W.H.F., Sandwell, D.T., 1997. Global seafloor topography from satellite altimetry and ship depth soundings. Science 277, 1957–1962.
Snyder, M.A., Sloan, L.C., Diffenbaugh, N.S., Bell, J.L., 2003. Future climate change and upwelling in the California Current. Geophys. Res. Lett. 30, 1823, http://dx.doi.org/10.1029/2003GL017647.
Takahashi, T., Sutherland, S.C., Wanninkhof, R., Sweeney, C., Feely, R.A., Chipman, D.W., Hales, B., Friederich, G., Chavez, F., Watson, A., Bakker, D.C.E., Schuster, U., Metzl, N., Yoshikawa-Inoue, H., Ishii, M., Midorikawa, T., Nojiri, Y., Sabine, C., Olafsson, J., Arnarson, S., Tilbrook, B., Johannessen, T., Olsen, A., Bellerby, R., Krtzinger, A., Steinhoff, T., Hoppema, M., de Baar, H.J.W., Wong, C.S., Delille, B., Bates, N.R., 2009. Climatological mean and decadal changes in surface ocean pCO_2, and net sea–air CO_2 flux over the global oceans. Deep Sea Res. Part II 56, 554–577.
Thomas, A.C., Carr, M.-E., Strub, P.T., 2001. Chlorophyll variability in eastern boundary currents. Geophys. Res. Lett. 28 (18), 3421–3424.
Wanninkhof, R., 1992. Relationship between gas exchange and wind speed over the ocean. J. Geophys. Res. 97, 7373–7381.
Wroblewski, J.S., 1977. A model of phytoplankton plume formation during variable Oregon upwelling. J. Mar. Res. 35, 357–394.